IEEE Access
Multidisciplinary | Rapid Review | Open Access Journal

Received 3 November 2025, accepted 13 November 2025, date of publication 17 November 2025,
date of current version 21 November 2025.

Digital Object Identifier 10.1109/ACCESS.2025.3633558

RESEARCH ARTICLE

Anomalous Reflectors Using 2-Bit Coding Metasurfaces Under Oblique Incidence for Millimeter-Wave Applications

EHSAN FAROKHIPOUR[1], (Member, IEEE), MOHAMMAD AMIN CHAYCHI ZADEH[2], SAJJAD ZOHREVAND[3], ANDREAS RENNINGS[1], (Member, IEEE), VAHID NAYYERI[2], (Senior Member, IEEE), NADER KOMJANI[3], AND DANIEL ERNI[1], (Member, IEEE)

[1]General and Theoretical Electrical Engineering (ATE), Faculty of Engineering, Center for Nanointegration Duisburg-Essen (CENIDE), University of Duisburg-Essen, 47048 Duisburg, Germany
[2]School of Advanced Technologies, Iran University of Science and Technology, Tehran 16846-13114, Iran
[3]Department of Electrical Engineering, Iran University of Science and Technology, Tehran 16846-13114, Iran

Corresponding author: Ehsan Farokhipour (ehsan.farokhipour@uni-due.de)

This work was supported in part by the Deutsche Forschungsgemeinschaft (DFG) through CRC/TRR 196 MARIE (Project-ID 287022738) under Project S03; in part by the Ministry of Culture and Science of the State of North Rhine-Westphalia (MKW NRW) through Project terahertz.NRW; and in part by the Federal Ministry of Education and Research, Germany (BMBF) through the 6GEM Research Hub under Grant 16KISK039.

ABSTRACT This paper presents the design, simulation, and experimental validation of six passive anomalous reflectors using 2-bit digital coding metasurfaces (DCMs) that can enable quasi-continuous single-beam steering for 5G n257 mm-wave applications. The design starts with a square-shaped meta-atom illuminated by a plane wave under an oblique incidence of $-45°$, enabling four discrete reflection phases with 90° phase increments. Each metasurface is constructed using identical meta-atoms in one direction and specific coding sequences in the orthogonal direction. Each supercell may contain equal or unequal numbers of meta-atoms per phase state, achieving anomalous reflections in the desired directions. As a demonstration, the design goals are six passive anomalous reflectors that produce six beams directed at $-32°$, $-17°$, $-7°$, $+7°$, $+17°$, and $+32°$. An expanded angular range with a minimal step size is also achieved by varying the frequency of the incident oblique beam. The full-wave simulations show good agreement with the analytical predictions. The far-field received power is measured across 27.5–29.5 GHz and compared to that of a perfect electric conductor (PEC). The measured frequency responses closely match those of the simulations, confirming the effectiveness of the proposed structures. These results are intended to facilitate a practical solution for wide-angle single-beam steering for mm-wave wireless communications with obstructed line-of-sight (LOS).

INDEX TERMS Anomalous reflection, digital coding metasurfaces, phase-gradient, oblique incidence, single-beam steering, millimeter-wave applications.

I. INTRODUCTION

Fifth-generation (5G) millimeter-wave (mm-wave) frequencies have attracted considerable attention in recent years because of their potential applications in advanced wireless communication systems for both indoor and outdoor environments, offering enhanced performance and functionality [1], [2], [3]. These applications leverage the unique advantages of mm-waves—namely, large available bandwidth and short wavelengths—which enable miniaturization of components, improved spatial resolution, and high-speed data transmission [4], [5], [6]. However, several challenges must

The associate editor coordinating the review of this manuscript and approving it for publication was Ladislau Matekovits.

be addressed to ensure the practical deployment of mm-wave communications, including free-space signal attenuation, limited coverage range, and strong sensitivity to obstacles, all of which can degrade signal reliability [7], [8], [9]. To address these issues, researchers are actively developing innovative solutions to improve signal robustness and extend the operational range [10].

Metasurfaces, the two-dimensional counterparts of bulk metamaterials, have emerged as powerful tools for manipulating electromagnetic (EM) waves in unprecedented ways, particularly at mm-wave frequencies [11], [12], [13]. They have proven effective in optimizing the wireless communication channels in complex propagation environments, especially finding practical applications in the emerging fields of intelligent reflecting surface (IRS) [14] and reconfigurable intelligent surface (RIS) [15]. A phase-gradient metasurface consists of an array of subwavelength meta-atoms engineered to impart spatially varying phase shifts to incident waves, thereby enabling wavefront control based on generalized Snell's law [16], [17]. This allows metasurfaces to support diverse functionalities such as beam steering, focusing, and wave shaping [18]. In reflective configurations, metasurfaces can also help compensate for radiation loss by redirecting incoming energy toward the desired directions to provide connectivity for non-line-of-sight (NLOS) communications by precisely controlling the reflection phase and amplitude. Once a meta-atom is conceptualized and designed, its complex reflection response can serve as a building block for metasurfaces that can realize engineered anomalous reflection behaviors [19], [20], [21].

In 2014, Cui et al. introduced digital coding metasurfaces (DCMs) as a novel design approach for discrete phase control at the meta-atom level [22]. In n-bit DCMs, meta-atoms are designed to produce reflection phases quantized in increments of $2\pi/2^n$, enabling a wide range of functionalities such as beam splitting [23], [24], [25], radar cross section (RCS) reduction [26], and beam scanning [27], [28]. The simplest case is 1-bit coding, in which two meta-atoms with a 180° phase difference are used. However, the beam manipulation capability of 1-bit DCMs is limited due to high quantization phase errors [29]. In contrast, 2-bit DCMs offer four discrete states with 90° phase increments, allowing finer phase control and improved single-beam scanning performance [30], [31], [32]. In [31] and [32], 2-bit coding metasurfaces were demonstrated under normal incidence based on the generalized Snell's law to achieve anomalous reflection. However, in those designs, the cluster size of each meta-atom within a supercell is fixed—meaning each phase state is repeated equally—which restricts angular resolution due to the direct relationship between the supercell size and reflection angle.

To date, most reported anomalous reflectors using DCMs have been designed under normal incidence [22], [23], [24], [25], [26], [27], [29], [30], [31], [32], [33], [34], [35], [36]. However, in real-world environments, incident waves frequently arrive at oblique angles, and thus additional considerations are needed when designing metasurfaces for oblique incidence to fully exploit their potential [37], [38], [39], [40], [41]. Despite recent progress, there is still a need to investigate reflective DCMs under oblique incidence conditions to achieve wide-angle, wideband single-beam steering in practical applications. None of the aforementioned studies have evaluated the beam squint phenomenon, which refers to a frequency-dependent shift in the main beam direction.

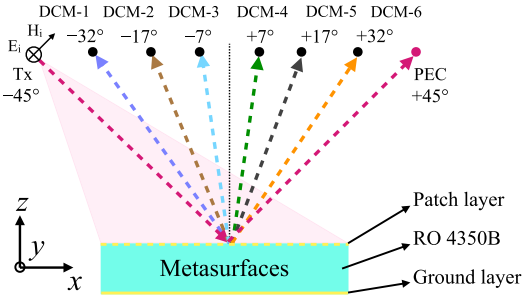

FIGURE 1. Schematic representation of beam steering using digital coding metasurfaces under an obliquely incident plane wave at −45°.

In this paper, we propose six passive anomalous reflectors using 2-bit DCMs designed under an oblique plane wave incidence of −45° to achieve reflections in the desired directions. Each metasurface comprises a 60 × 60 array of identical meta-atoms arranged along one direction, with specific coding sequences applied along the orthogonal direction. As a demonstration, the design goals in this study are six anomalous reflectors that generate six beams directed at −32°, −17°, −7°, +7°, +17°, and +32°. The beam squint phenomenon is also investigated for each structure, which enables a finer angular resolution through frequency tuning. Finally, six separate metasurfaces were designed, fabricated, and measured. Each panel produces one narrow beam at its prescribed angle, and the measured received powers agree well with the full-wave simulations.

II. DESIGN AND PRINCIPLE

Fig. 1 depicts the representation of beam steering using digital coding metasurfaces (DCMs) under a −45° y-polarized incident plane wave. Each metasurface generates a single anomalously reflected beam steered toward a specific angle. The structure consists of a dielectric substrate (RO4350B) with a thickness of 0.5 mm, relative permittivity of 3.55, and loss tangent of 0.0027, sandwiched between a bottom metallic ground layer and a patterned top metallic patch layer. Metasurface performance is evaluated using an antenna array model based on distinct coding sequences.

A general metasurface of size $M \times N$ meta-atoms is considered. According to the array factor formulation, the far-field pattern under an arbitrary incidence is given by [39]:

$$F(\theta_r, \phi_r) = \sum_{m=1}^{M}\sum_{n=1}^{N} \exp\Big(-j\Big(\Phi(m,n) + k_0 P_x (m-0.5)\big[\sin\theta_r \cos\phi_r + \sin\theta_i \cos\phi_i\big]$$

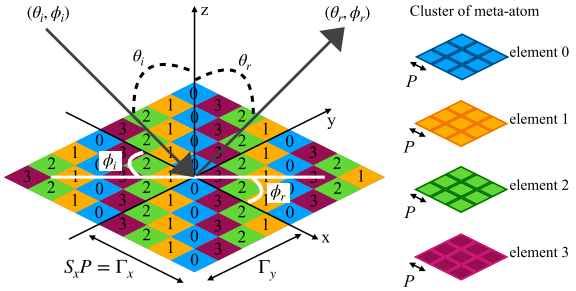

FIGURE 2. Illustration of generalized Snell's law for a 2-bit reflective metasurface under arbitrary incidence, demonstrating anomalous reflection.

$$+ k_0 P_y (n-0.5)\left[\sin\theta_r \sin\phi_r + \sin\theta_i \sin\phi_i\right]\Big)\Big), \tag{1}$$

where (θ_i, ϕ_i) and (θ_r, ϕ_r) denote the elevation and azimuth angles of the incidence and reflection, respectively. $P_x = P_y = P$ is the meta-atom period, k_0 is the free-space wave vector, and $\Phi(m, n)$ represents the phase of the (m, n)-th meta-atom. For 2-bit coding, $\Phi(m, n) = 0, \pi/2, \pi$, or $3\pi/2$ corresponds to coding states 0-3.

Fig. 2 illustrates the generalized Snell's law for a reflective metasurface under arbitrary incidence, showing that the reflection angle is determined by the phase-gradient, incidence angle and operating frequency. When the metasurface consists of a finite number of meta-atoms, the maximum of $|F(\theta_r, \phi_r)|$ in (1) occurs at angles $\theta_{r,s}$ satisfying [42]:

$$\theta_{r,s} = \arcsin\left(s\lambda_0\sqrt{\frac{1}{\Gamma_x^2} + \frac{1}{\Gamma_y^2}} - \sin\theta_i\right) \tag{2}$$

where $s = 0, \pm 1, \ldots$ and $\Gamma_x = S_xP$ and $\Gamma_y = S_yP$, as shown in Fig. 2, are the physical periods along the x- and y-directions, respectively. To form the phase-gradient DCM, meta-atoms with identical phase values are arranged along the x-axis, while specific 1D coding sequences are applied along the y-axis. In this study, all metasurfaces are invariant along y, i.e., $\Gamma_y \to \infty$, and the main beam corresponds to $s = -1$. The first-order diffraction angle becomes:

$$\theta_{r,-1} = \arcsin\left(\frac{-\lambda_0}{\Gamma_x} - \sin\theta_i\right) \tag{3}$$

For $\theta_i = -45°$, the radiation condition of the main beam is considered to be within $\theta_i < \theta_{r,-1} < \theta_s$, where $\theta_s = 45°$ is the specular reflection angle, corresponding to $\Gamma_x \to \infty$. At 28 GHz, this yields $\Gamma_x > 7.57$ mm. Given the meta-atom period $P = 2.15$ mm, the minimum valid value of Γ_x is $4P = 8.6$ mm, corresponding to a lower limit of $\theta_{r,-1} = -32°$.

In this study, CST Studio is used to design meta-atoms and perform full-wave simulations under oblique incidence using the finite-difference time-domain (FDTD) method. MATLAB facilitates the rapid computation of gradient distributions and far-field responses. Finally, Ansys HFSS simulates the metasurfaces under the excitation of a standard horn antenna using the hybrid finite element-boundary integral (FEBI) method, optimizing both computational accuracy and resource efficiency.

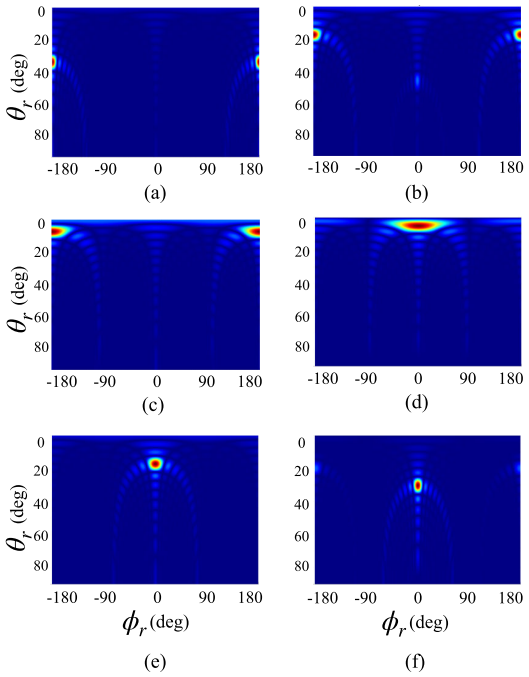

FIGURE 3. Analytically predicted normalized radiation patterns at 28 GHz, showing steering at different angles for (a) DCM-1 through (f) DCM-6.

III. ANALYTICAL AND NUMERICAL SIMULATIONS

The design and analysis of the proposed DCMs are performed using both analytical modeling and full-wave simulations. To validate the design, we set the operating frequency to $f = 28$ GHz (within the 5G n257 mm-wave band), with the incident wave defined by $\theta_i = -45°$, and the digital coding level set to $n = 2$. In our design, each structure consists of 60×60 subwavelength square meta-atoms, with a total size of $12\lambda_0 \times 12\lambda_0$ at 28 GHz.

A. ANALYTICAL RESULTS

As established in the previous section, the lower steering limit is $-32°$ with $S_x = 4$. Based on this, additional supercell sizes are selected with $S_x = 5$, 6, 8, 12, and 28, which result in reflected angles at $-17°$, $-7°$, $+7°$, $+17°$, and $+32°$, respectively. The proposed design can be extended beyond the six demonstrated cases. Next, we investigate six anomalous reflectors obtained from the determined supercell sizes with distinct 2-bit coding sequences. The 1D coding sequences of each DCM within its determined S_x are defined as follows:

- Code 1: 0123…$(S_x = 4)$
- Code 2: 01123…$(S_x = 5)$
- Code 3: 001223…$(S_x = 6)$
- Code 4: 00112233…$(S_x = 8)$
- Code 5: 000111222333…$(S_x = 12)$
- Code 6: 000000011111112222222333333…$(S_x = 28)$

Codes 1, 4, 5, and 6 feature equal repetitions of elements 0–3, resulting in equal cluster sizes per phase state.

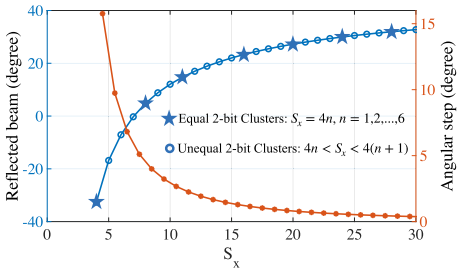

FIGURE 4. Reflected beam angle and angular step size as a function of supercell size in terms of number of meta-atoms at 28 GHz.

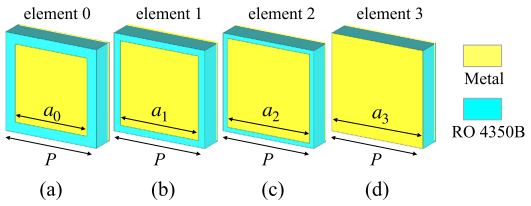

FIGURE 5. Structure of 2-bit meta-atom in four states: (a) element 0, (b) element 1, (c) element 2, (d) element 3. All dimensions in mm: $P = 2.15$, $a_0 = 1.70$, $a_1 = 1.88$, $a_2 = 1.95$, $a_3 = 2.15$.

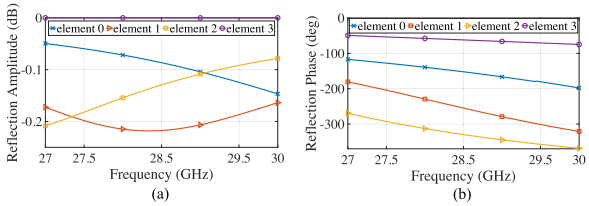

FIGURE 6. Simulated (a) reflection amplitude and (b) reflection phase response of the meta-atom in each 2-bit state under −45° plane wave incidence.

In contrast, Codes 2 and 3 use unequal repetitions of the coding elements within a supercell. This implies that the cluster size for each phase state can be independently selected according to the desired supercell size, which does not affect the main beam direction. The reflected beam can be steered in finer angular increments by selectively varying the cluster size assigned to each phase state.

Fig. 3 presents the analytically predicted normalized far-field radiation patterns, showing the distinct beam directions achieved via different coding sequences. To further illustrate the angular steering capability enabled by varying the supercell size, Fig. 4 shows the relationship between the number of meta-atoms in the supercell (S_x) and the resulting reflected beam angle $\theta_{r,-1}$. By incrementally increasing S_x from 4 to 28, the reflected beam can be tuned across a range of −32° to +32°. Notably, the associated angular step size is non-uniform, as shown on the right axis of Fig. 4. These increments become progressively smaller with increasing S_x—transitioning from coarse steps at smaller S_x to much finer steps at larger S_x.

B. FULL-WAVE SIMULATION RESULTS

The geometry of the 2-bit square-shaped meta-atoms is illustrated in Fig. 5. Each meta-atom has a period $P = 2.15$ mm

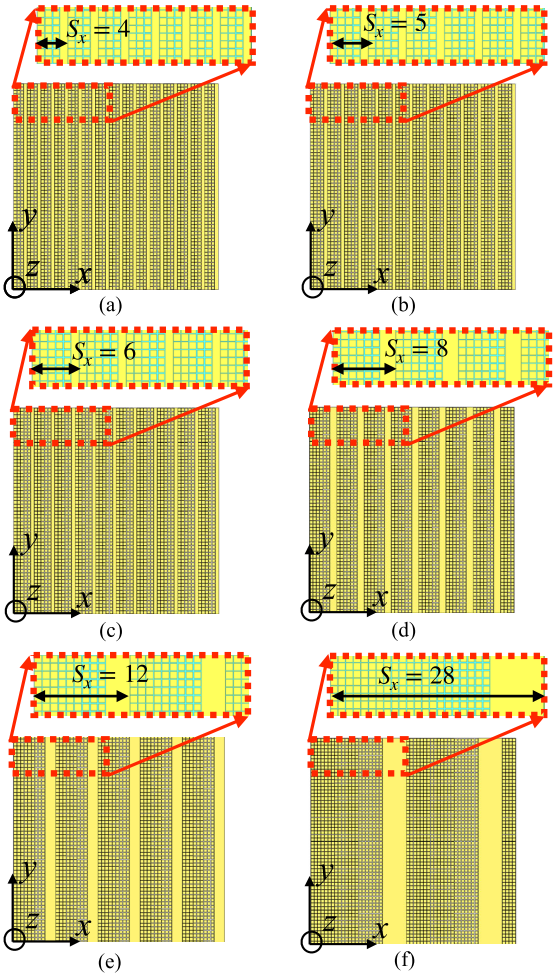

FIGURE 7. Full DCM configurations and zoom-in views of 1D coding sequences for (a) DCM-1 with Code 1 through (f) DCM-6 with Code 6.

($\approx 0.2\lambda_0$ at 28 GHz), with a metallic patch over an RO4350B substrate and a PEC ground plane. By varying the square patch width from a_0 to a_3, 90° phase shifts of 0°, 90°, 180°, 270° at the designed frequency are realized. As shown in Fig. 6, CST simulations under a −45° y-polarized incidence confirm that these phase states are achieved with phase errors within ±20° across 27.5–29.5 GHz. The reflection amplitude exceeds −0.21 dB for all states across the band. The designed meta-atoms are polarization-sensitive due to their non-isotropic structure under the oblique incidence, resulting in a larger reflection phase error between the coding states. This larger phase error could be unsuitable for a 2-bit coding strategy at the metasurface level. The derived analytical phase profiles are then used to generate full metasurface layouts. Fig. 7 shows the physical layouts of all six structures. Fig. 8 shows the simulated far-field radiation patterns of all metasurfaces using CST under −45° oblique plane wave excitation. In all cases, single-beam radiation is observed with weak specular reflection at +45°, attributed to PEC backing (not accounted for in the analytical model). The phase error effects on the overall radiation performance, such as beam pointing and the presence of undesirable grating lobes,

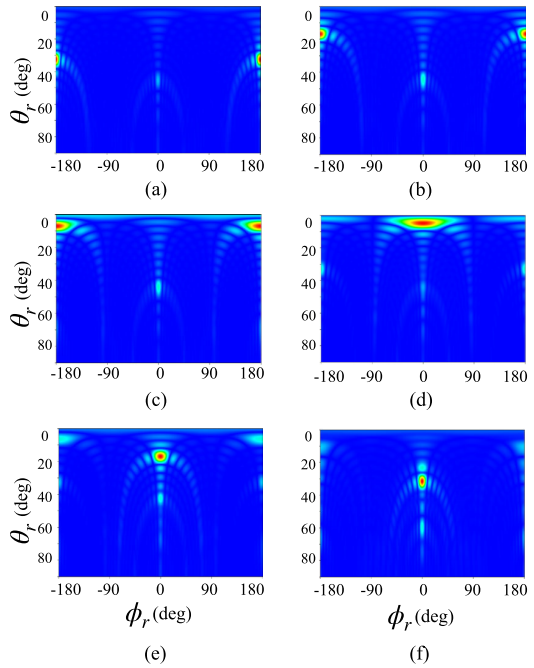

FIGURE 8. CST-simulated far-field radiation patterns at 28 GHz for (a) DCM-1 with Code 1 through (f) DCM-6 with Code 6.

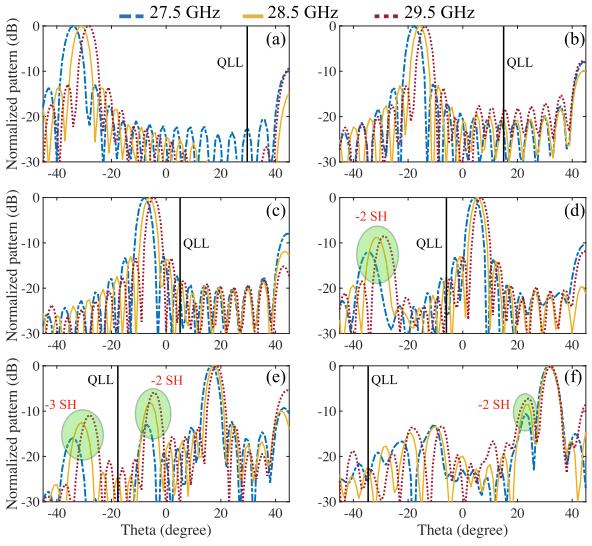

FIGURE 9. Frequency-dependent far-field radiation patterns for all DCMs showing beam squint effect: (a)–(f) correspond to DCM 1–6.

can also be observed. Noted that DCM-1 serves as the first equal cluster configuration that steers the reflected beam to $-32°$. Similarly, DCM-4, also employing equal clusters, redirects the beam to $+7°$. To achieve intermediate beam steering angles between these discrete values, DCM-2 and DCM-3 utilize coding with unequal cluster sizes. Specifically, DCM-2 steers the beam to $-17°$, whereas DCM-3 directs it to $-7°$.

Table 1 summarizes the analytical and simulated beam steering angles and performance metrics of the metasurfaces. The small angular differences in beam pointing of the

TABLE 1. Simulated Performance of the DCMs for Different θ_r.

DCM	Supercell Size Γ_x	Reflection @ 28 GHz Analytical	Reflection @ 28 GHz Numerical	Squint	QLL (dB) @ 28.5 GHz	SLL (dB) @ 28.5 GHz
1	8.6 mm ($\approx 0.8\lambda_0$)	$-31.5°$	$-32°$	6.1°	-30	-14.5
2	10.75 mm ($\approx 1.0\lambda_0$)	$-16.4°$	$-17°$	4.4°	-21.5	-10.0
3	12.9 mm ($\approx 1.2\lambda_0$)	$-6.6°$	$-7°$	4.1°	-18.0	-11.8
4	17.2 mm ($\approx 1.6\lambda_0$)	$+6.5°$	$+7°$	3.5°	-17.6	-9.1
5	25.8 mm ($\approx 2.4\lambda_0$)	$+16.3°$	$+17°$	2.3°	-24.8	-8.3
6	60.2 mm ($\approx 5.6\lambda_0$)	$+31.4°$	$+32°$	1.2°	-24.4	-8.7

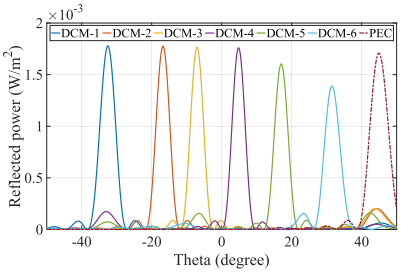

FIGURE 10. Comparison of the reflected power for the metasurfaces and a PEC of the same size at 28 GHz to calculate the directional efficiency.

predicted and the simulated far-field radiation patterns could be attributed to the phase error and mutual coupling effects in the actual structures, which are not considered in the analytical model. The results confirm excellent agreement between the predicted and simulated beam directions, with squint reduction as the supercell size increases. This is also visualized in Fig. 9, where the beam direction shifts with frequency owing to the squint. The figure shows that in addition to spatial coding, varying the frequency of the obliquely incident beam provides a secondary degree of control, allowing even finer angular steps in beam steering. Smaller supercell sizes result in a higher sensitivity to wavelength changes, whereas larger Γ_x values produce more stable beams.

Quantization lobe level (QLL) and sidelobe level (SLL) are also reported in Table 1. The QLL is defined as a local peak near $-\theta_r$, while SLL represents the maximum sidelobe excluding QLL. The half-power beamwidth (HPBW) ranges from 4.3° to 5.1° across codes. Specular reflection at 45° is at least 10 dB lower than the main beam at 28.5 GHz. In some cases, an elevated SLL is due to higher-order space harmonics (SH) that arise between the incident direction and main beam.

The directional efficiency of a reflective metasurface at a given frequency is defined as the ratio of the power reflected from the metasurface in its intended steering direction to the specularly reflected power from a perfect electric conductor (PEC) of the same size [34]:

$$\eta = \frac{P_r^{\mathrm{MS}}}{P_r^{\mathrm{PEC}}} \times 100\% \tag{4}$$

where P_r^{MS} and P_r^{PEC} denote the power reflected from the metasurface collected in the main lobe direction and the specularly reflected power from the PEC reference surface, respectively. To evaluate the directional efficiency numerically, the reflected power at 28 GHz for each of the

TABLE 2. Comparison of some features of the proposed work with similar other designs.

Ref.	Mode / Incidence	Bandwidth	Bit Num.	Layer Num.	Cell Num.	Beam Direction (°)	Single Beam	QLL (dB)	Continuous Beam Steering	Reconfiguration
[31]	Reflective / normal	5.85-6 GHz	1-bit	1	60×60	±30	No	–	N.A.	Passive
[31]	Reflective / normal	5.85-6 GHz	2-bit	1	60×60	30	Yes	N.A.	N.A.	Passive
[23]	Transmissive / normal	10.4–11.2 GHz	1-bit	1	8×8	±22, ±32, ±49	No	–	N.A.	Passive
[35]	Reflective / normal	11.1 GHz	1-bit	1	40×40	±7.9, ±16.2	No	–	N.A.	Active
[37]	Reflective / oblique	300 GHz	1-bit	1	36×36	15, 48	Yes	N.A.	N.A.	Active
[34]	Reflective / normal	530-730 GHz	2-bit	1	64×64	38	Yes	N.A.	N.A.	Passive
[36]	Reflective / normal	7.2 GHz	2-bit	1	16×16	−30	Yes	−11	N.A.	Active
[43]	Reflective / normal	35-43 GHz	prephased 1-bit	1	20×20	−15, 15, 30	Yes	−7.5	N.A.	Passive
[44]	Reflective / normal	34.3 to 49.9 GHz	prephased 1-bit	2	20×20	0, 15, 30	Yes	−9.8	N.A.	Passive
Here	**Reflective / oblique**	**27.5-29.5 GHz**	**2-bit**	**1**	**60×60**	**-32, -17, -7 7, 17, 32**	**Yes**	−19	**Yes**	**Passive**

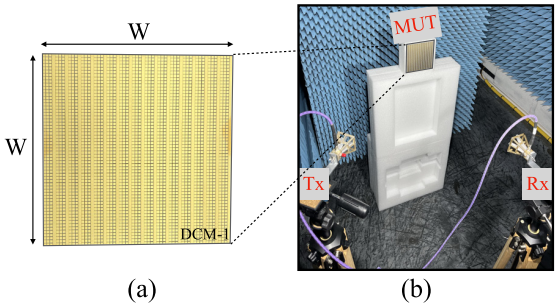

FIGURE 11. (a) Photograph of one of the fabricated reflectors with $12\lambda_0 \times 12\lambda_0$ size. (b) Measurement setup inside the anechoic chamber.

six proposed structures, as well as for a PEC reference of identical dimensions, is shown in Fig. 10.

Notably, the reflected power peaks at the main lobe directions of DCM 1–4 surpass the specular reflection from the PEC, resulting in directional efficiencies above 100%. Values exceeding unity do not violate energy conservation. They indicate a more focused redistribution of the incident power in the desired non-specular direction than the redirected power from the PEC in the specular direction. This enhanced directional efficiency highlights the effectiveness of the structures in concentrating the reflected energy in specific angular regions. Conversely, DCM-5 and DCM-6 exhibit reflected power peaks below that of the PEC, leading to reduced directional efficiencies. This decline primarily stems from the larger supercell sizes, resulting in fewer supercells fitting within the fixed aperture, thus reducing the angular concentration and peak intensity of the reflected power in the main beam direction.

IV. EXPERIMENTAL VALIDATION

A. MEASUREMENTS

To experimentally validate the analytical and numerical results, prototypes of all six proposed metasurfaces were fabricated and tested in an anechoic chamber. Fig. 11(a) shows a photograph of one of the fabricated metasurfaces, each with a physical size of $12\lambda_0 \times 12\lambda_0$ at 28 GHz.

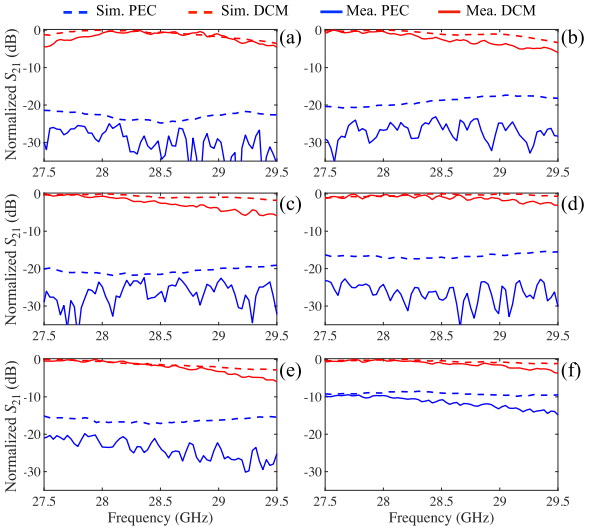

FIGURE 12. Normalized measured and simulated S_{21} between Tx and Rx horn antennas for each DCM and the PEC reference under −45° oblique incidence at (a) −32°, (b) −17°, (c) −7°, (d) +7°, (e) +17°, and (f) +32°.

Fig. 11(b) illustrates the experimental setup for measuring the reflected power. The setup includes a metasurface under test (MUT) and two QRH40 horn antennas, one for transmission (Tx) and one for reception (Rx), connected to a vector network analyzer. The phase centers of both horns are aligned with the center of the MUT. A separation distance of 60 cm ($\approx 56\lambda_0$) is maintained between the MUT and antennas to ensure far-field conditions. The Tx horn antenna remains fixed, providing a constant oblique incidence angle of −45° during the characterization. The Rx horn is repositioned according to the anomalous reflection characteristics of each metasurface, ensuring that it captures the redirected beam in the correct direction.

To evaluate the beam steering performance, a perfect electric conductor (PEC) of the same size as the metasurface is used as a reference. Each MUT is tested under the same −45° oblique incidence, and the reflected power is measured at its respective steering angle: −32°, −17°, −7°, +7°,

+17°, and +32°. Fig. 12 shows the normalized measured and simulated S_{21} responses between the Tx and Rx horns for each case, across 27.5–29.5 GHz. The results are achieved using the FEBI method in HFSS, which offers computational efficiency for full-wave simulations. The results confirm that the metasurfaces outperform the PEC in directing energy toward the intended angles, validating their functionality.

Across all cases, the gain variation within the frequency band is approximately 3.5 dB. Minor frequency offsets between the measurements and simulations are observed and can be attributed to fabrication tolerances, misalignment, and measurement errors. At higher frequencies, discrepancies may also arise because of differences in conductor and dielectric losses of the materials in simulation and fabrication, and alignment inaccuracies during the measurement, which are neglected in the simulations. These experimental results confirm the practical viability of the proposed structures for real-world deployment in mm-wave wireless systems that require passive and directional beam control.

B. DISCUSSION

Table 2 provides a comparison between this study and recent related studies on digital coding metasurfaces in terms of some key performance parameters, including, angle of incidence, number of bit coding, QLL, and angular beam steering performance. The works in [23], [31], and [35] rely on 1-bit coding for reflective and transmissive metasurfaces but do not achieve single-beam radiation under normal incidence. While [31], [34], and [36] also introduce 2-bit metasurfaces capable of single-beam steering, they are limited to a discrete angular step. In contrast, the 1-bit coding metasurfaces exploiting an integrated phase change material (PCM) in [37] support single-beam steering by increasing the incident angle from 0° to 75°, but with limited angular flexibility. The works in [43] and [44] propose prephased 1-bit metasurfaces for single-beam generation under normal incidence. However, they require more complex implementations, including multilayer stacks and complex 2D prephase distributions, in which the unit cell phases are randomly predetermined before being controlled by one bit. Compared with the 2-bit coding metasurface, the prephased 1-bit coding structure has a lower gain and a higher QLL owing to the larger phase quantization error. Notably, [44] requires two dielectric substrates, three copper layers, and an air gap to achieve a 90° prephase shift.

In comparison, the reflective metasurfaces proposed here offer 2-bit operation, wide-angle coverage, single-beam radiation, low QLL, and practical implementation under oblique incidence, making them suitable for next-generation mm-wave applications. Unlike the reported works using DCM in the literature that have been studied under a standard normal incidence, anomalous reflectors of this study have been investigated under a more practical oblique incidence of −45°. Our reflectors are based on a 2-bit coding strategy with a lower phase quantization error compared to the 1-bit coding. This finer phase quantization minimizes phase errors across the aperture, leading to a reduced QLL of −19 dB for all six reflectors, which is much lower than that typically observed in 1-bit coding designs. The finer beam resolution in the angular range from −32° to 32° is achieved due to our specific coding strategy that is enabled by unequal cluster sizes of meta-atoms per phase state. The passive approach in our work leverages the geometric flexibility of unequal cluster sizes per phase state within a 2-bit 1D coding supercell. As a demonstration, six passive anomalous reflectors using DCM are designed to generate single beams directed at −32°, −17°, −7°, +7°, +17°, and +32°.

Passive DCM can play a crucial role in the development of a reconfigurable intelligent surface (RIS) for modern wireless communication systems. The anomalous reflection from an arbitrary incidence into an arbitrary desired direction based on passive DCM is key to coverage enhancement through RIS to provide connectivity for NLOS scenarios [45], [46]. The design of a programmable supercell using an integrated active material could be suitable for realizing dynamic beam control through an active platform with fewer active elements [47]. This can be an implication of this study, which may inspire the design of a programmable supercell compared with those on the meta-atom level to reduce the active components of the RIS for mm-wave beam steering applications.

V. CONCLUSION

This paper presents six passive anomalous reflectors using 2-bit phase-gradient digital coding metasurfaces (DCMs) under an oblique incidence of −45°. Each reflector produces single-beam radiation pointing at a specific angle for 5G n257 mm-wave applications. Each structure was constructed by placing identical meta-atoms along one axis and applying tailored 1D coding sequences along the orthogonal axis to control the beam direction. The performance of the proposed reflectors was validated through analytical modeling, full-wave simulations, and experimental measurements. The measured frequency responses of the received power closely matched the simulation results, confirming the ability to redirect incident waves efficiently in the desired directions. These passive reflectors can enhance signal coverage for 5G mm-wave communications in NLOS scenarios.

Furthermore, the successful design and validation of the proposed passive DCMs under oblique incidence not only advances the state-of-the-art for static continuous beam steering using the unequal cluster concept but also could establish a pathway towards RIS realization by designing a programmable supercell. It is noted that while the size of the meta-atoms could remain unchanged, the size of the supercell could be modified by varying the number of subwavelength meta-atoms. Moving from a subwavelength meta-atom level towards a comparable or even larger than operating wavelength supercell level programmability could significantly reduce hardware complexity by decreasing the number of active elements. This approach would facilitate continuous beam steering through programmable supercell exploiting unequal cluster with reduced number of active

components than full-array reconfiguration at the meta-atom level.

REFERENCES

[1] W. Hong, K.-H. Baek, and S. Ko, "Millimeter-wave 5G antennas for smartphones: Overview and experimental demonstration," *IEEE Trans. Antennas Propag.*, vol. 65, no. 12, pp. 6250–6261, Dec. 2017.

[2] T. S. Rappaport, Y. Xing, G. R. MacCartney, A. F. Molisch, E. Mellios, and J. Zhang, "Overview of millimeter wave communications for fifth-generation (5G) wireless networks—With a focus on propagation models," *IEEE Trans. Antennas Propag.*, vol. 65, no. 12, pp. 6213–6230, Dec. 2017.

[3] M. Xiao, S. Mumtaz, Y. Huang, L. Dai, Y. Li, M. Matthaiou, G. K. Karagiannidis, E. Björnson, K. Yang, I. Chih-Lin, and A. Ghosh, "Millimeter wave communications for future mobile networks," *IEEE J. Sel. Areas Commun.*, vol. 35, no. 9, pp. 1909–1935, Sep. 2017.

[4] Z. A. Pandit Jibran, M. Kalaagi, D. Seetharamdoo, and C. Maye, "Reflective anomalous beam splitter (RABS) metasurface for millimeter-wave (mm-Wave) frequency," *J. Appl. Phys.*, vol. 136, no. 2, Jul. 2024, Art. no. 024902.

[5] M. Elkashlan, T. Q. Duong, and H.-H. Chen, "Millimeter-wave communications for 5G: Fundamentals: Part I [Guest editorial]," *IEEE Commun. Mag.*, vol. 52, no. 9, pp. 52–54, Sep. 2014.

[6] A. Franzese, R. Negra, A. Malignaggi, N. Maletic, B. Sutbas, and C. Carta, "28-GHz SiGe bidirectional 4-element beamformer chip for 5G applications based on a 4-way ultracompact switchable power divider," *IEEE Trans. Microw. Theory Techn.*, vol. 72, no. 12, pp. 7050–7060, Dec. 2024.

[7] X. Lin and J. G. Andrews, "Connectivity of millimeter wave networks with multi-hop relaying," *IEEE Wireless Commun. Lett.*, vol. 4, no. 2, pp. 209–212, Apr. 2015.

[8] A. Benoni, F. Capra, M. Salucci, and A. Massa, "Toward real-world indoor smart electromagnetic environments—A large-scale experimental demonstration," *IEEE Trans. Antennas Propag.*, vol. 71, no. 11, pp. 8450–8463, Nov. 2023.

[9] G. Oliveri, F. Zardi, and A. Massa, "On the improvement of the performance of inexpensive electromagnetic skins by means of an inverse source design approach," *IEEE Trans. Antennas Propag.*, vol. 73, no. 5, pp. 3284–3295, May 2025.

[10] Á. F. Vaquero, E. Martinez-De-Rioja, M. Arrebola, J. A. Encinar, and M. Achour, "Smart electromagnetic skin to enhance near-field coverage in mm-Wave 5G indoor scenarios," *IEEE Trans. Antennas Propag.*, vol. 72, no. 5, pp. 4311–4326, May 2024.

[11] C. L. Holloway, E. F. Kuester, J. A. Gordon, J. O'Hara, J. Booth, and D. R. Smith, "An overview of the theory and applications of metasurfaces: The two-dimensional equivalents of metamaterials," *IEEE Antennas Propag. Mag.*, vol. 54, no. 2, pp. 10–35, Apr. 2012.

[12] M. Qu, Q. Du, T. Lan, C. Wang, J. Su, and V. Nayyeri, "Wideband high-intensity self-bending Bessel-like beam metasurface-based launcher for wireless applications," *IEEE Trans. Microw. Theory Techn.*, vol. 72, no. 11, pp. 6349–6359, Nov. 2024.

[13] J. Huang and J. A. Encinar, *Reflectarray Antennas*. Hoboken, NJ, USA: Wiley, 2007.

[14] C. Li, M. van Delden, A. Sezgin, T. Musch, and Z. Han, "IRS-assisted MISO system with phase noise: Channel estimation and power scaling laws," *IEEE Trans. Wireless Commun.*, vol. 22, no. 6, pp. 3927–3941, Jun. 2023.

[15] J. Li, L. Yang, W. Hao, I. Ahmad, H. Liu, F. Shu, and D. Niyato, "Multi-layer transmitting RIS-aided receiver for collaborative jamming and anti-jamming networks," *IEEE Trans. Wireless Commun.*, vol. 24, no. 8, pp. 6518–6534, Aug. 2025.

[16] N. Yu, P. Genevet, M. A. Kats, F. Aieta, J.-P. Tetienne, F. Capasso, and Z. Gaburro, "Light propagation with phase discontinuities: Generalized laws of reflection and refraction," *Science*, vol. 334, no. 6054, pp. 333–337, Oct. 2011.

[17] W. Barnard, J. W. Odendaal, and J. Joubert, "Anomalous reflection from a phase gradient metasurface with arbitrary incident angle," *IEEE Access*, vol. 11, pp. 18385–18390, 2023.

[18] Z. Li, J. Liu, J. Zhang, L. Shao, C. Zhang, X. Wang, R. Jin, and W. Zhu, "Shaping electromagnetic fields with irregular metasurface," *Adv. Mater. Technol.*, vol. 7, no. 9, Sep. 2022, Art. no. 2200035.

[19] A. Díaz-Rubio and S. A. Tretyakov, "Macroscopic modeling of anomalously reflecting metasurfaces: Angular response and far-field scattering," *IEEE Trans. Antennas Propag.*, vol. 69, no. 10, pp. 6560–6571, Oct. 2021.

[20] D. Kong, T. D. Phan, J. Palosaari, J. Juuti, A. Pärssinen, and P. J. Soh, "A simplified method for designing highly efficient reflective metasurfaces with wide steering angles," *IEEE Antennas Wireless Propag. Lett.*, vol. 23, pp. 3664–3668, 2024.

[21] R. Wang, Y. Yang, B. Makki, and A. Shamim, "A wideband reconfigurable intelligent surface for 5G millimeter-wave applications," *IEEE Trans. Antennas Propag.*, vol. 72, no. 3, pp. 2399–2410, Mar. 2024.

[22] T. J. Cui, M. Q. Qi, X. Wan, J. Zhao, and Q. Cheng, "Coding metamaterials, digital metamaterials and programmable metamaterials," *Light: Sci. Appl.*, vol. 3, no. 10, p. e218, Oct. 2014.

[23] K. K. Katare, S. Chandravanshi, A. Biswas, and M. J. Akhtar, "Realization of split beam antenna using transmission-type coding metasurface and planar lens," *IEEE Trans. Antennas Propag.*, vol. 67, no. 4, pp. 2074–2084, Apr. 2019.

[24] E. Farokhipour, A. Rennings, and D. Erni, "Digital-coding reconfigurable metasurface for THz anomalous reflections based on liquid crystal," in *Proc. Int. Conf. Mobile Miniaturized Terahertz Syst. (ICMMTS)*, Feb. 2025, pp. 1–4.

[25] L. Liang, M. Qi, J. Yang, X. Shen, J. Zhai, W. Xu, B. Jin, W. Liu, Y. Feng, C. Zhang, H. Lu, H.-T. Chen, L. Kang, W. Xu, J. Chen, T. J. Cui, P. Wu, and S. Liu, "Anomalous terahertz reflection and scattering by flexible and conformal coding metamaterials," *Adv. Opt. Mater.*, vol. 3, no. 10, p. 1311, Oct. 2015.

[26] C. Fu, L. Han, C. Liu, X. Lu, and Z. Sun, "Combining Pancharatnam–Berry phase and conformal coding metasurface for dual-band RCS reduction," *IEEE Trans. Antennas Propag.*, vol. 70, no. 3, pp. 2352–2357, Mar. 2022.

[27] S. Liu, T. J. Cui, Q. Xu, D. Bao, L. Du, X. Wan, W. X. Tang, C. Ouyang, X. Y. Zhou, H. Yuan, H. F. Ma, W. X. Jiang, J. Han, W. Zhang, and Q. Cheng, "Anisotropic coding metamaterials and their powerful manipulation of differently polarized terahertz waves," *Light, Sci. Appl.*, vol. 5, no. 5, Jan. 2016, Art. no. e16076.

[28] G. Bashir, A. K. Singh, and A. Dubey, "Wide band beam steering digital metasurface reflectarray antenna for millimeter wave applications," *IEEE Access*, vol. 11, pp. 121800–121810, 2023.

[29] M. Jia, C. Zhao, Z. Tang, Z. Jin, N. Zhang, and X. Han, "Continuous manipulation of electromagnetic radiation based on ultrathin flexible frequency coding metasurface," *Sci. Rep.*, vol. 14, no. 1, p. 18915, Aug. 2024.

[30] J. Guo, D. Guan, S. Yu, X. Su, and Z. Liu, "A novel amplitude–phase synthesis method for metasurface-based radar target HRRP imitation," *IEEE Trans. Microw. Theory Techn.*, vol. 73, no. 10, pp. 8094–8105, May 2025.

[31] R. Malleboina, J. C. Dash, and D. Sarkar, "Design of anomalous reflectors by phase gradient unit cell-based digitally coded metasurface," *IEEE Antennas Wireless Propag. Lett.*, vol. 22, pp. 2305–2309, 2023.

[32] S. E. Hosseininejad, K. Rouhi, M. Neshat, A. Cabellos-Aparicio, S. Abadal, and E. Alarcón, "Digital metasurface based on graphene: An application to beam steering in terahertz plasmonic antennas," *IEEE Trans. Nanotechnol.*, vol. 18, pp. 734–746, 2019.

[33] F. Ahmed, T. Hassan, N. Melouki, H. Naseri, P. PourMohammadi, A. Iqbal, and T. A. Denidni, "A multibit and frequency-reconfigurable reflecting surface for RIS applications," *IEEE Antennas Wireless Propag. Lett.*, vol. 23, pp. 653–657, 2024.

[34] S. Iqbal, A. Noor, N. Ullah, Y. Saifullah, S. Ahmed, M. S. Nisar, and S.-W. Wong, "Polarization insensitive non-interleaved frequency multiplexed dual-band terahertz coding metasurface for independent control of reflected waves," *Sci. Rep.*, vol. 14, no. 1, p. 21199, Sep. 2024.

[35] H. Yang, X. Cao, F. Yang, J. Gao, S. Xu, M. Li, X. Chen, Y. Zhao, Y. Zheng, and S. Li, "A programmable metasurface with dynamic polarization, scattering and focusing control," *Sci. Rep.*, vol. 6, no. 1, p. 35692, Oct. 2016.

[36] C. Huang, B. Sun, W. Pan, J. Cui, X. Wu, and X. Luo, "Dynamical beam manipulation based on 2-bit digitally-controlled coding metasurface," *Sci. Rep.*, vol. 7, no. 1, p. 42302, Feb. 2017.

[37] E. Farokhipour, A. Rennings, and D. Erni, "Digital-coding based on a phase-change material for optically preconfigurable metasurfaces," in *Proc. IEEE Conf. Antenna Meas. Appl. (CAMA)*, Genoa, Italy, Nov. 2023, pp. 995–998.

[38] M. Yazdi and M. Albooyeh, "Analysis of metasurfaces at oblique incidence," *IEEE Trans. Antennas Propag.*, vol. 65, no. 5, pp. 2397–2404, May 2017.
[39] J. Kappa, Z. Dang, D. Sokoluk, and M. Rahm, "Analysis of coding metasurfaces for incident radiation at oblique incidence angles," *OSA Continuum*, vol. 2, no. 7, pp. 2172–2180, Jun. 2019.
[40] M. Albooyeh, S. Kruk, C. Menzel, C. Helgert, M. Kroll, A. Krysinski, M. Decker, D. N. Neshev, T. Pertsch, C. Etrich, C. Rockstuhl, S. A. Tretyakov, C. R. Simovski, and Y. S. Kivshar, "Resonant metasurfaces at oblique incidence: Interplay of order and disorder," *Sci. Rep.*, vol. 4, no. 1, p. 4484, Mar. 2014.
[41] T. Kim, S. Lee, S. Oh, J. Kim, J. Oh, and S. Choi, "Pre-phased 1-bit reflective passive metasurface with optimum number of pre-phasing for low QLL and SLL at 140 GHz," *IEEE Trans. Antennas Propag.*, vol. 73, no. 2, pp. 975–985, Feb. 2025.
[42] X. G. Zhang, W. X. Tang, W. Jiang, G. D. Bai, J. Tang, L. Bai, C. Qiu, and T. J. Cui, "Light-controllable digital coding metasurfaces," *Adv. Sci.*, vol. 5, no. 11, Nov. 2018, Art. no. 1801028.
[43] Q. Wu, X. Long, J. Yin, C. Yu, H. Wang, and W. Hong, "Single-layer 1-bit prephased single-beam metasurface using true-time delayed unit cells," *IEEE Antennas Wireless Propag. Lett.*, vol. 21, pp. 1095–1099, 2022.
[44] J. Yin, Q. Wu, Q. Lou, H. Wang, Z. N. Chen, and W. Hong, "Single-beam 1 bit reflective metasurface using prephased unit cells for normally incident plane waves," *IEEE Trans. Antennas Propag.*, vol. 68, no. 7, pp. 5496–5504, Jul. 2020.
[45] J. Q. Han, X. J. Ma, H. Yi, S. C. Tian, H. X. Liu, L. Li, and T. J. Cui, "Indoor non-line-of-sight millimeter-wave coverage enhancements by field-reorganizable passive digital coding metasurfaces," *Adv. Photon. Res.*, vol. 4, no. 11, Nov. 2023, Art. no. 2300188.
[46] M. K. T. Al-Nuaimi, S.-L. Zhu, R.-S. Chen, G.-L. Huang, and A. A. Kishk, "Wideband passive electromagnetic skin assisted 5G base station in urban areas at mmWave," *IEEE Antennas Wireless Propag. Lett.*, vol. 24, pp. 1–5, 2025.
[47] S. Kosulnikov, X. Wang, and S. A. Tretyakov, "Discrete-impedance metasurfaces for wireless communications in D-band," *IEEE Trans. Antennas Propag.*, vol. 72, no. 1, pp. 591–599, Jan. 2024.

EHSAN FAROKHIPOUR (Member, IEEE) received the B.Sc. degree in electrical engineering-communication from the Shahid Bahonar University of Kerman, Kerman, Iran, in 2015, and the M.Sc. degree in electrical engineering-electromagnetic fields and waves from Iran University of Science and Technology, Tehran, Iran, in 2018. From 2019 to 2021, he was a Research Assistant with the Millimeter-Wave Research Laboratory, Iran University of Science and Technology. Since 2022, he has been a member of the Laboratory of General and Theoretical Electrical Engineering, University of Duisburg-Essen. His research interests include manipulation of EM waves, on-chip antennas, beam steering techniques, leaky-wave antennas, metasurfaces, and lens-based systems for millimeter-wave/sub-THz applications.

MOHAMMAD AMIN CHAYCHI ZADEH was born in Tabriz, Iran, in 1987. He received the B.Sc. degree in electrical engineering from the University of Tabriz, in 2009, and the M.Sc. and Ph.D. degrees in electrical engineering from Iran University of Science and Technology (IUST), Tehran, in 2013 and 2024, respectively. He is currently a Postdoctoral Researcher with the Advanced Radio Communication Systems Laboratory (ARCS Lab), IUST, where he focuses on the development of next-generation antenna systems and electromagnetic structures. He is also actively engaged in the design and development of active and passive microwave circuits and subsystems. His research interests encompass the design and analysis of planar and conformal microstrip antennas, metamaterials and metasurfaces, complex electromagnetic media, and leaky-wave antennas.

SAJJAD ZOHREVAND was born in Tehran, Iran, in 1996. He received the B.Sc. degree in electrical engineering from the Islamic Azad University South Tehran Branch (IAUSTB), Tehran, in 2019, and the M.Sc. degree in electrical engineering from Iran University of Science and Technology (IUST), Tehran, in 2022. He is currently a Research Assistant with the Millimeter-Wave Research Laboratory, IUST. His research interests include planar and conformal antennas, the holographic principle, reconfigurable intelligent surfaces (RISs), metasurfaces and metamaterials, as well as plasmonic and spoof plasmonic.

ANDREAS RENNINGS (Member, IEEE) received the Dipl.-Ing. and Dr.-Ing. degrees from the University of Duisburg-Essen, Germany, in 2000 and 2008, respectively.

He carried out his diploma work during a stay with the University of California, Los Angeles. He studied electrical engineering with the University of Duisburg-Essen. From 2006 to 2008, he was with IMST GmbH, Kamp-Lintfort, Germany, where he was an RF Engineer. Since then, he has been a Senior Scientist and the Principal Investigator with the Laboratory for General and Theoretical Electrical Engineering, University of Duisburg-Essen. His general research interests include all aspects of theoretical and applied electromagnetics, currently with a focus on medical applications and on-chip millimeter-wave/THz antennas.

Dr. Rennings has received several awards, including the Student Paper Price at the 2005 IEEE Antennas and Propagation Society International Symposium and the VDE-Promotionspreis 2009 for the dissertation.

VAHID NAYYERI (Senior Member, IEEE) was born in Tehran, Iran, in 1983. He received the B.Sc. degree in electrical engineering from Iran University of Science and Technology (IUST), Tehran, in 2006, the M.Sc. degree in electrical engineering from the University of Tehran, Tehran, in 2008, and the Ph.D. degree from IUST, in 2013.

From 2007 to 2013, he was a Research Assistant with IUST and a Visiting Scholar with the University of Waterloo, Waterloo, ON, Canada. In 2013, he joined the Faculty with IUST, where he is currently an Associate Professor, the Director of the Advanced Radio Circuits and Systems (ARCS) Laboratory, and the Head of the Department of Satellite Technology. In 2019, he also a Visiting Professor with the University of Waterloo. He has co-authored more than 150 technical articles and two books/book chapters. His research interests include microwave active and passive circuits, as well as applied and computational electromagnetics.

Dr. Nayyeri received the Best Ph.D. Thesis Award from the IEEE Iran Section, in 2014 and the Raj Mittra Travel Grant from the IEEE Antennas and Propagation Society, in 2024. He was a recipient of several institutional honors from IUST, including the Outstanding Educator Award, the Distinguished Research Faculty Award, and the International Excellence Award. He serves as an Associate Editor for both IEEE TRANSACTIONS ON MICROWAVE THEORY AND TECHNIQUES and *IET Microwaves, Antennas and Propagation*. He has been actively involved in the IEEE Iran Section, where he has served as a member for the Board of Directors and the Chair of both the Membership Development and the Young Professionals Committees.

NADER KOMJANI received the B.Sc., M.Sc. and Ph.D. degrees in electrical engineering from Iran University of Science and Technology, Iran, in 1988 and 1991, and 2000, respectively. He is currently an Associate Professor with Iran University of Science and Technology. He has taught microstrip antennas, communication systems, advanced engineering mathematics and electromagnetic courses, since 1998. His area of interests include UWB and multiband microstrip antennas, numerical methods in electromagnetic, phased array antennas and passive and active microwave systems.

DANIEL ERNI (Member, IEEE) received the Diploma degree in electrical engineering from the University of Applied Sciences Rapperswil (OST), Rapperswil-Jona, Switzerland, in 1986, and the Diploma degree in electrical engineering and the Ph.D. degree in laser physics from ETH Zürich, Zürich, Switzerland, in 1990 and 1996, respectively.

Since 1990, he has been with the Laboratory for Electromagnetic Fields and Microwave Electronics (IFH), ETH Zürich. From 1995 to 2006, he was the Founder and the Head of the Communication Photonics Group, ETH Zürich. Since October 2006, he has been a Full Professor with the Laboratory for General and Theoretical Electrical Engineering, University of Duisburg-Essen, Duisburg, Germany. From 2017 to 2018, he was with the Institute of Electromagnetic Fields (IEF), ETH Zürich, as a Visiting Professor. He is currently a Co-Founder of the spin-off company airCode, Duisburg, working on flexible printed RFID technology. His current research interests include optical interconnects, nanophotonics, plasmonics, ultra-sensitive optical biosensing, advanced solar cell concepts, optical and electromagnetic metamaterials, RF, mm-wave and THz engineering, chipless flexible RFIDs, biomedical engineering, bioelectromagnetics, marine electromagnetics, computational electromagnetics, multiscale and multiphysics modeling, numerical structural optimization, and science and technology studies (STS).

Dr. Erni is a fellow of the Electromagnetics Academy and a member of the Center for Nanointegration Duisburg-Essen (CENIDE), as well of Materials Chain, the Flagship Program of the University Alliance Ruhr, of Electrosuisse, the Swiss Physical Society (SPS), the German Physical Society (DPG), and the Optical Society of America (OPTICA).